

S.T. Yau High School Science Award (Asia)

2020

**Ti6Al4V Microstructure Image Segmentation with Computer
Vision Analysis**

Registration Number: Comp-036

Member 1: Xin Wenkang, Nanyang Junior College, Singapore

Member 2: Wong Zi Hao, Deston, Nanyang Junior College, Singapore

Member 3: Hoo Di Heng, Nanyang Junior College, Singapore

Supervising Teacher: Dr Nathaniel Ng, Institute of High Performance Computing,
Agency for Science, Technology and Research, Singapore

Teacher Mentor: Mr Goh Kien Soon, Nanyang Junior College, Singapore

August 30, 2020

Abstract

Many important mechanical properties of materials, such as strength and hardness, depend on their microstructural features. There is hence a need to quantify the microstructural features, such as phase volume fraction and average grain size, quickly and accurately from a microstructure image. Manual identification by materials scientists is often slow and labour intensive and suffers from poor repeatability. Therefore, digital image processing techniques, such as the watershed transform, are often deployed to automate the task by dividing the microstructure images into areas containing each individual microstructural feature so that data about the microstructural characteristics can be extracted. However, watershed transform is prone to oversegmentation, a situation where the image is too finely divided into segmented regions. In this report, we propose using fast Fourier transform (FFT) and frequency domain operations to improve the reliability of watershed transform. We develop a systematic procedure to process a microstructural image for effective segmentation and demonstrate the possibility of the following microstructural data collection. We verify the effectiveness of our approach on two microstructure image of titanium alloy, a type of alloy widely used in industries.

Keywords— Microstructure analysis, Fast Fourier transform, Watershed transform, Titanium alloy, Computer vision

Contents

| | | |
|----------|--|-----------|
| 1 | Introduction | 3 |
| 2 | Computer Vision Analysis | 4 |
| 2.1 | Denoising and Thresholding | 5 |
| 2.2 | Fast Fourier Transform | 6 |
| 2.3 | Watershed Transform | 8 |
| 3 | Reducing Oversegmentation | 9 |
| 4 | Data Extraction | 9 |
| 5 | Results and Discussion | 12 |
| 6 | Comparison with Existing Techniques | 14 |
| 6.1 | Comparison with Manual Measurement | 14 |
| 6.2 | Comparison with Techniques Used by Previous Research | 15 |
| 6.2.1 | Canny Edge Detection | 15 |
| 6.2.2 | MIPAR Software | 15 |
| 7 | Conclusion | 16 |
| 8 | Acknowledgement | 17 |

2020 S.-T. Yau High School Science Award

List of Figures

| | | |
|----|---|----|
| 1 | Image analysis workflow | 4 |
| 2 | Microstructure images used | 5 |
| 3 | Gaussian blurring | 6 |
| 4 | Otsu thresholding | 6 |
| 5 | Fast Fourier transform | 7 |
| 6 | FFT-processed image | 8 |
| 7 | Segmentation of IMRE image | 10 |
| 8 | Segmentation of section of IMRE image | 11 |
| 9 | Reducing oversegmentation | 11 |
| 10 | Segmentation of section of MIPAR image | 13 |
| 11 | Comparison with Canny edge detection on IMRE image | 20 |
| 12 | Comparison with Canny edge detection on section of IMRE image | 21 |
| 13 | Comparison with MIPAR on IMRE image | 22 |
| 14 | Comparison with MIPAR on MIPAR image | 23 |

List of Tables

| | | |
|---|---|----|
| 1 | IMRE image data | 13 |
| 2 | MIPAR image data | 14 |
| 3 | Comparison of phase volume fraction measurement | 14 |

2020 S.-T. Yau High School Science Award

1 Introduction

Ti6Al4V is widely used in industries due to its high strength-to-weight ratio and strong resistance to corrosion. Many such mechanical properties are claimed to be dependent on the microstructural features of the alloy [1]. The popularity of Ti6Al4V, particularly within high value manufacturing sectors such as aerospace, often makes it the subject of microstructural analysis. Ti6Al4V, as a two-phase material, demonstrates a wide variety of different microstructural features, making research developed for Ti6Al4V more likely to be applicable to other materials [2].

Several techniques, both manual and automatic, have been proposed to quantify microstructural features of a microstructure image. The American Society for Testing and Materials (ASTM) E112 standard suggests a manual procedure to measure the average grain size of metals [3]. Several lines are drawn across the image and any interception with grain boundaries is marked. The average number of interceptions per unit length gives an approximation of the average grain size. Random placement of lines avoids bias, but aspect ratio of grains could not be measured. Manually placing the lines along the length and width of each grain gives a more accurate measurement, but may result in biased results [2]. The labour intensive nature of such undertakings undermines the reliability and repeatability of the data collected.

A few automatic procedures have been developed to analyse the microstructure image. It is recognised that the most crucial step is obtaining an accurate segmentation of the image that effectively isolate individual grains [4]. Subsequent data extraction becomes straightforward once segmentation is successfully conducted. Tiley et al. [5] and Collins et al. [6] deployed Photoshop and its extension Fovea Pro to quantify microstructure features in Titanium alloys. Yang and Liu [7] proposed using Canny edge detection algorithm for segmentation of an image that has been denoised with a Gaussian blurring filter, before using Image-P Plus software for data collection. Sosa et al. [4] developed a software system called MIPAR to automatically measure several microstructural features. The software is able to use the fast Fourier transform of a microstructure image and conduct frequency domain operations to improve the quality of image, so as to improve the quality of the subsequent segmentation. Campbell et al. [2] utilised edge detection algorithms to identify the boundaries of grains. Markers are placed in the centre of closed boundaries to improve subsequent watershed transform. Campbell et al. also proposed a region-merging algorithm to reduce oversegmentation.

However, there are certain limitations in the existing techniques. Edge detection algorithms used by Yang and Liu and Campbell et al. are prone to noise in the image caused by different factors such as uneven illumination, leading to less reliable results. Edge de-

tection is also less reliable when the boundary between the foreground and the background is unclear due to lower contrast between the two areas' intensity. Fast Fourier transform in MIPAR developed by Sosa et al. is only used to address the problem of milling artefact, while it can be further utilised to identify edges and improve segmentation results. The commercial nature of both MIPAR and Fovea Pro may discourage researchers from adopting them and being closed-source software, they may be difficult to customise for different scenarios. Our approach uses Python and its open-source libraries, including OpenCV and Numpy, to automatically process microstructural images. The open-source nature of our system makes it more versatile and simple to verify and customise. This report proposes using fast Fourier transform, in addition to other processing techniques, to extract certain desired features of an image. This report also develops several simple algorithms to demonstrate the possibility of subsequent data collection, though the main focus is on effective segmentation, which is the most critical step to achieve reliable quantification of the microstructural features [2] [4].

2 Computer Vision Analysis

We present a systematic procedure to process and analyse a Ti6Al4V microstructure image using Python and OpenCV, an open-source computer vision library. The workflow is shown in Figure 1.

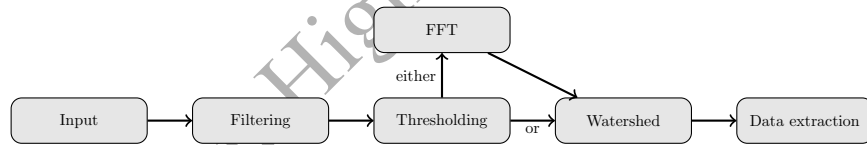
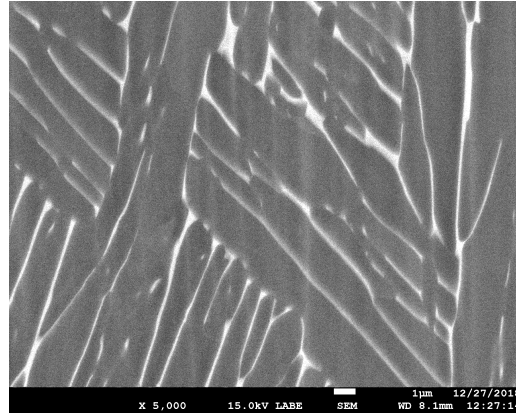
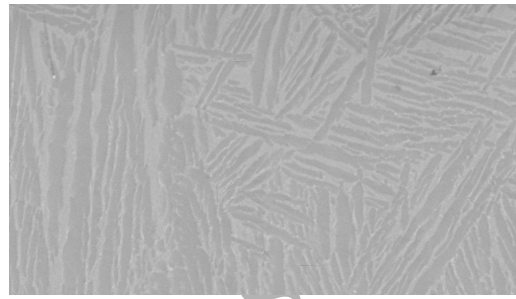


Figure 1: Image analysis workflow

To achieve effective segmentation with watershed transform, it is important to obtain a clean, binarised image while preserving the edges in the image before segmentation. Therefore, a wide range of techniques is adopted, including filtering, thresholding and fast Fourier transform, to process the image before implementing the watershed transform. Subsequent data extraction can be conducted using the labelled image produced by watershed transform. The effectiveness of our approach is tested on two microstructural images. One image is provided by material scientists from A*STAR's Institute of Materials Research and Engineering (IMRE). It is a backscattered electron image taken with a field-emission scanning electron microscope (FESEM). The other one is provided by MIPAR software. We shall denote the former IMRE image and the latter MIPAR image (Figure 2).



(a)



(b)

Figure 2: Microstructure images used in this report where (a) image provided by IMRE (b) image provided by MIPAR

2.1 Denoising and Thresholding

The initial raw image is filtered to reduce noise that will cause oversegmentation at later stages. Several well-known image filtering techniques are tested, including the median filter, the bilateral filter and the Gaussian blurring (Figure 3). Generally, a technique that will preserve the edge features of the image while denoising is preferred. For our image, Gaussian blurring is found to be the most successful among the techniques tested, in agreement with previous research [2] [7].

The image is then thresholded and binarised. Among the various thresholding techniques available in OpenCV, Otsu's method [8] proves to be the most effective. Otsu's method automatically calculates the optimal global threshold that will best separate the foreground pixels from the background ones, creating two classes of pixels. The algorithm attempts to find a single intensity threshold that minimises the inter-class variance. In scanning electron microscope images, there is a clear distinction between the gray scale

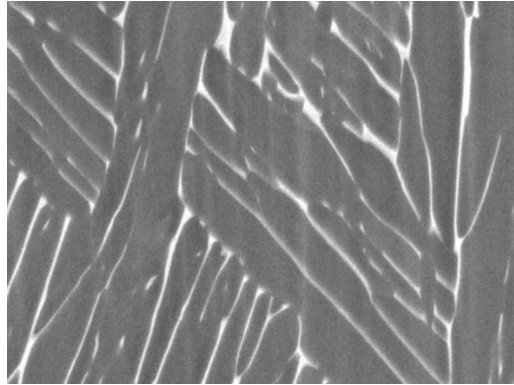


Figure 3: Filtered image using Gaussian blurring with a 5×5 kernel.



Figure 4: Thresholded image using Otsu's method

intensities of the grains and the background, as pointed out by previous research [7]. Therefore, the intensity histogram of the image shows clear peaks for the foreground and the background pixels. Otsu's method can hence produce a cleaner, binarised image effectively with a single global threshold (Figure 4).

2.2 Fast Fourier Transform

After the thresholding, the image still may not be suitable for watershed transform due to oversegmentation caused by noises in the image. One additional processing step is introduced to improve the reliability of watershed transform, through the use of fast Fourier transform (FFT). FFT converts the binary image from its spatial domain to the frequency domain, so as to allow for frequency domain operations on the image to extract specific features and reduce noise. The processed frequency image is then converted back to the spatial domain with an inverse Fourier transform. The FFT transform $F(x, y)$ of

a M by N image, which is represented by a function $f(m, n)$, is given by Equation 1:

$$F(x, y) = \sum_{m=0}^{M-1} \sum_{n=0}^{N-1} f(m, n) e^{-i2\pi(x\frac{m}{M} + y\frac{n}{N})} \quad (1)$$

Conversely, with the frequency domain image represented by a function $F(x, y)$, its inverse Fourier transform is given by Equation 2:

$$f(m, n) = \frac{1}{MN} \sum_{m=0}^{M-1} \sum_{n=0}^{N-1} F(x, y) e^{i2\pi(x\frac{m}{M} + y\frac{n}{N})} \quad (2)$$

Sharp intensity changes, which occur in the boundary regions in the image, correspond to high frequencies in the frequency image [9]. The direction along with such transitions occur dictate the orientation of the high frequency parts in the frequency image [4]. A mask is applied onto the FFT image to select such frequencies in an effort to retain the edge features. Figure 5 shows the FFT of the previous thresholded image.

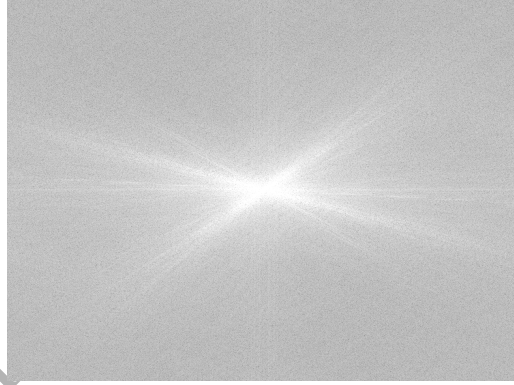


Figure 5: Fast Fourier transform of the thresholded image

Notice that there are spikes along certain directions. The spikes are frequencies that represent the boundary pixels in the original image where the intensity experiences a sharp change. To extract these frequencies, a mask defined by two parameters θ and Δy is used to extract each spike. θ determines the angle of the mask while Δy determines the width of the mask:

$$F(x, y) = \begin{cases} F(x, y) & \text{if } \frac{N-\Delta y}{2} + \tan(\theta)(x - \frac{M}{2}) \leq y \leq \frac{N-\Delta y}{2} + \tan(\theta)(x - \frac{M}{2}) \\ 0 & \text{otherwise} \end{cases} \quad (3)$$

After applying several masks along certain directions, a frequency image with only the desired frequencies preserved is obtained. The processed frequency image is then converted back to its spatial domain using the inverse Fourier transform. An image with clearer, sharper edges is obtained (Figure 6), and it is able to minimise oversegmentation during the eventual watershed transform.

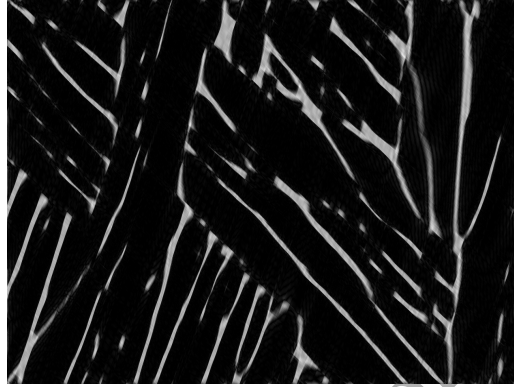


Figure 6: FFT-processed image

2.3 Watershed Transform

Watershed transform is adopted to segment the image. With watershed transform, the image is taken as a topographical relief and flooded [10]. Sources are situated at local minima, and when floods from two regions meet, a 'dam' is built to prevent mixing of the floods. Eventually, all the 'dams' indicate the boundary regions of the original image. However, due to the large number of minima points caused by noises in the image, watershed transform often suffers from oversegmentation [11]. Apart from denoising the image, using a marker-based watershed transform also helps to improve the segmentation result [12]. A marker indicates the desired locations where flooding should take place, so as to minimise oversegmentation. The method has been proven successful by applications in other areas [13] [14] [15].

Distance transform and connected components analysis are deployed to generate the markers. If a FFT-processed image is used, it must be first thresholded to obtain a binary image. Using an OpenCV function, the distance transform of the image is obtained. The distance transform assigns each pixel of an image with its distance to the nearest background pixel [16]. This means that pixels nearer to the centre of each grain have a higher value compared other pixels. Therefore, thresholding the distance transform with an appropriate threshold yields the foreground area of the image, which represent the central part of the grains. The boundary area is then identified by subtracting the

morphological dilation of the FFT-processed image with the foreground area.

Connected components analysis is then used to label each foreground area in the thresholded distance transform image with a unique integer [17]. This labelled image is used as the marker for watershed transform. The marker-based watershed transform algorithm provided by OpenCV takes the FFT-processed image and the marker as input, and returns an image with grains pixels labelled with unique integers starting from 2, background with 1 and boundaries with -1. Extracting only the boundary pixels' locations and colouring corresponding pixels in the original BSE image provides us with a segmented microstructural image. Segmentation results on full and cropped IMRE images are shown in Figure 7 and 8.

3 Reducing Oversegmentation

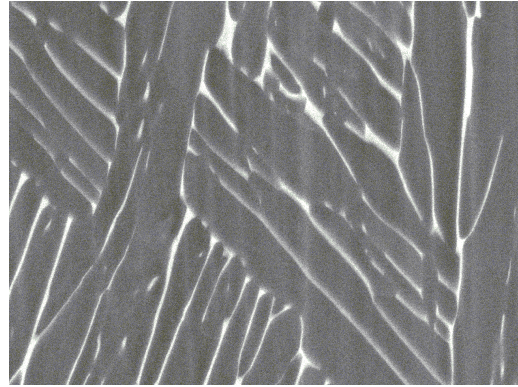
The labelled image produced by watershed transform may exhibit oversegmentation, as shown in Figure 7c. The oversegmentation can be reduced by altering parameters for the watershed transform, but sometimes the problem persists after testing with several sets of parameters. Therefore, an algorithm is introduced to reduce oversegmentation by region merging. Noting that the oversegmented parts are often small, area is used as the selection criterion for merging regions. Labelled regions that have areas below a predetermined threshold are merged with their surrounding regions. The images before and after reducing oversegmentation are shown in Figure 9.

Composite merging criteria, such as the one used in [2], can be developed according to the type of oversegmentation shown in different images.

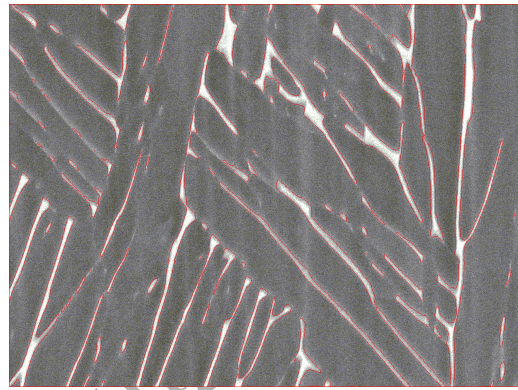
4 Data Extraction

For this section, we demonstrate the possibility of data extraction from the labelled image produced in the previous section. We shall focus on a section of the image, such as the one in Figure 8 for this section and the following result analysis.

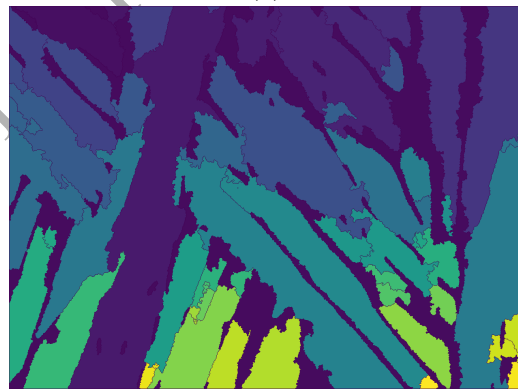
The output labelled image (Figure 8c) of the watershed transform can be viewed as a m by n matrix, represented by $m(x, y)$, with integer elements. It can be used to facilitate data extraction from the microstructural image. Area of each grain is simply reflected by the total number of pixels labelled with the grain's corresponding unique integer. With the total area of grains, volume fraction of the alpha phase (low intensity foreground) and beta phase (high intensity background) can be computed since area fraction and volume fraction are taken as equivalent [18].



(a)



(b)



(c)

Figure 7: Segmentation results where (a) original IMRE image (b) segmentation of the image (c) labelled image

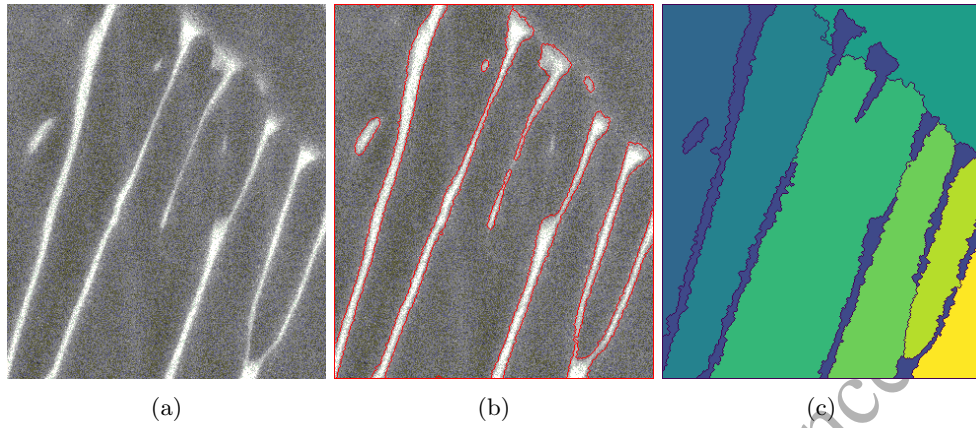


Figure 8: Segmentation results where (a) a section of the IMRE image (b) segmentation of the section (c) labelled image of the section

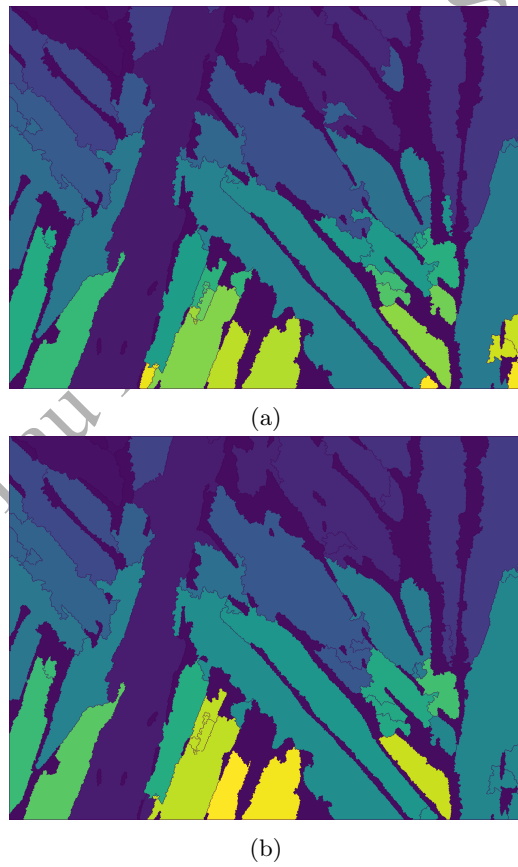


Figure 9: Results of reducing oversegmentation where (a) before reducing (b) after reducing

For the circumference of each grain, an algorithm is used to compute the number of boundary pixels of each grain, thus yielding the circumference. Every grain is labelled by an integer starting from 2. For each pixel labelled by an integer larger or equal to 2, the unique values in its eight neighbouring pixels can be retrieved. If this set of values contains -1, which represent the boundary pixels, this pixel is taken as one part of the circumference. For one particular grain, all pixels that have -1 as one of their neighbouring pixels are extracted and used to construct the circumference. The algorithm is repeated for each grain.

$$m(x, y) = \begin{cases} m(x, y) & \text{if } -1 \text{ is in its neighbouring pixels} \\ 0 & \text{otherwise} \end{cases} \quad (4)$$

To measure the width and length, and hence the size of each grain, an ellipse is fit to the region occupied by it. This is done with another OpenCV function, `cv2.fitEllipse`, which uses the algorithm developed by [19]. The estimated width and length of the grain is given by the length of the minor-axis and major-axis respectively. The average grain size is given by Equation 5, where L_n and D_n are the length and width of a grain respectively [2].

$$GS = \frac{L_n + D_n}{2} \quad (5)$$

It must be noted that all data collected is represented by numbers of pixels, which do not directly reflect the real values of the microstructural features. The area data, for example, represents the total amount of pixels in a certain grain. The real values can be deduced upon knowing the size of the digital image and the relevant data, such as magnification and aspect ratio, of the scanning instrument.

5 Results and Discussion

Now we present the results of our approach. Due to the limited dataset of this student project, we only have two microstructure images to work with. However, since the two images exhibit different image qualities and different microstructure features, they are able to reflect the effectiveness of our algorithm.

Figure 8b and 8c shows the segmentation result and the labelled image on a section of the IMRE image. Table 1 shows the data extracted from the labelled image.

Figure 10 shows another set of results based on a section of the MIPAR image. The data

| Grain no | Area | Circumference | Width | Length | Grain Size |
|----------|-------|---------------|-------|--------|------------|
| 1 | 16115 | 1137 | 17 | 43 | 30 |
| 2 | 21919 | 1350 | 78 | 407 | 243 |
| 3 | 12380 | 929 | 148 | 167 | 158 |
| 4 | 33017 | 1489 | 113 | 359 | 236 |
| 5 | 12580 | 946 | - | - | - |
| 6 | 6214 | 708 | 42 | 221 | 132 |
| 7 | 4460 | 435 | 68 | 130 | 99 |

Table 1: Data extracted from the segmentation result of IMRE image

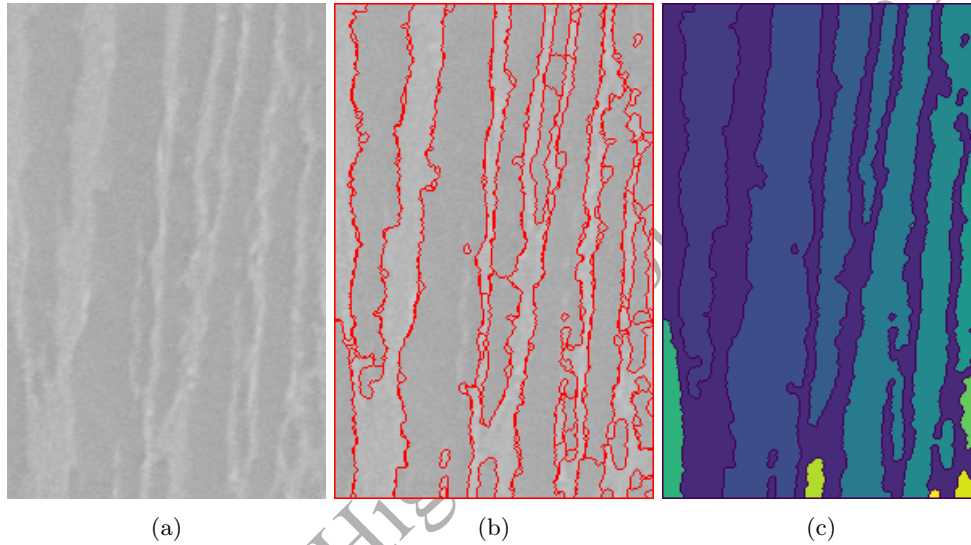


Figure 10: Segmentation results where (a) a section of a microstructure image from MIPAR (b) segmentation of the section (c) labelled image of the section

is shown in table 2.

Overall, our method achieved good segmentation result and a good labelled image on the IMRE image. Area and circumference data fits our expectation based on the relative size of the grains. The grain size data, however, is not satisfactory at times. For example, in Table 1, Grain 1 has a problematic length and width, while on Grain 5, the algorithm fails. The problem is more significant in Table 2. This could be due to the OpenCV function not working as expected when handling a shape with complex boundary features and overall shapes. However, the purpose of our algorithm is mainly demonstrative, and more accurate and flexible data extraction methods can be developed by future research.

| Grain no | Area | Circumference | Width | Length | Grain size |
|----------|-------|---------------|-------|--------|------------|
| 1 | 5542 | 724 | 36 | 243 | 140 |
| 2 | 11188 | 990 | 8 | 13 | 11 |
| 3 | 3937 | 717 | 21 | 262 | 142 |
| 4 | 1079 | 354 | 12 | 136 | 75 |
| 5 | 6667 | 1077 | 6 | 7 | 6 |
| 6 | 5568 | 1033 | 7 | 12 | 10 |
| 7 | 1234 | 371 | 14 | 141 | 78 |
| 8 | 1048 | 264 | 11 | 108 | 60 |
| 9 | 357 | 132 | 11 | 44 | 28 |
| 10 | 224 | 77 | 10 | 23 | 17 |
| 11 | 160 | 61 | 13 | 16 | 15 |

Table 2: Data extracted from the segmentation result of MIPAR image

6 Comparison with Existing Techniques

We further demonstrate the effectiveness of our approach with comparison to both manual and several automatic methods.

6.1 Comparison with Manual Measurement

Our method's measurement of phase volume fraction is compared with manual measurement. As suggested by ASTM E562 [18], the manual measurement uses the point count method for measuring phase volume fraction. A regular grid of points is superposed over the image and number of points that are inside the region of interest is noted. If the point is on the boundaries, one-half a 'hit' is counted. Then the total number of 'hits' divided by the total number of points gives the volume fraction of the phase of interest.

Table 3 shows the comparison of phase volume fraction measurement between our method and manual method.

| | α volume fraction | β volume fraction |
|---------------------------|--------------------------|-------------------------|
| Our method on IMRE image | 86.4% | 14.6% |
| Manual on IMRE image | 85.7% | 14.3% |
| Our method on MIPAR image | 60.7% | 39.3% |
| Manual on MIPAR image | 60.0% | 40.0% |

Table 3: Comparison of phase volume fraction measurement between our method and manual method

There is a good match between our method and manual method in both IMRE and MIPAR image, with our method's alpha volume fraction being 0.7% higher than manual

method in both images. This may be due to the subjectivity involved in manual measurement of the volume fraction. Since the manual method requires one to select points that are either in the alpha grain area or on the boundary, points that are located on less distinct boundary lines may be consistently left out during manual measurement, leading to a lower alpha volume fraction.

There is a significant reduction in the time taken to perform measurements using our image processing algorithm. The images shown in Figure 2a and 2b took an average of 3.79s to process, segment and quantify, far shorter than the measurement time needed for manual measurements of more than 15 minutes. Automatic methods like ours allow for a large quantity of microstructure images to be analysed within a short period of time. The automated nature of the algorithm also ensures repeatability.

6.2 Comparison with Techniques Used by Previous Research

6.2.1 Canny Edge Detection

The segmentation results of our method are compared with Canny edge detection, which is employed in [7] to achieve segmentation of alpha and beta grains in Ti6Al4V. Canny edge detection is also used in [2].

As shown in Figure 11 and 12, compared to Canny edge detection used in [7], our watershed transform achieved a better segmentation result on IMRE image with clearer and more complete boundary lines. Watershed transform also has the benefit of generating a connected component labelled image that will facilitate data extraction.

6.2.2 MIPAR Software

Lastly our method is compared against with the MIPAR software. MIPAR offers a variety of image processing tools for the user to analyse the image in a graphical user interface. MIPAR provides Gaussian filtering and thresholding, and an automatic watershed transform function. After filtering and thresholding, the watershed transform provided by MIPAR is used to segment our IMRE image and the image provided by MIPAR. The comparison with our method is shown in Figure 13 and 14.

It appears that our method achieves a slightly better result with less oversegmentation in the IMRE image. In the MIPAR image, however, our method has a less desirable outcome with some parts of the image not properly segmented. This may be anticipated as algorithms of MIPAR are better optimised for its own images. MIPAR software is equipped with a wide range of other functions which may help with the segmentation so the result shown does not represent the full potential of the software. Instead, the

comparison serves to demonstrate the usefulness of our approach in certain scenarios.

7 Conclusion

We have presented a systematic approach to automatically segment a microstructure image, using watershed transform and a variety of techniques that help to improve the segmentation result. Fast Fourier transform is used to allow for frequency domain operations that extract edge features in certain directions. We tested our method on two different microstructure images. An algorithm is developed to reduce oversegmentation. The overall segmentation results are mostly positive, while the labelled image produced by watershed transform may be less accurate in cases where the transition from foreground to background is not very clear. The efficiency advantage of our automated method over manual measurement is evident, while more sophisticated data extraction algorithm can be developed for more accurate quantification of microstructural features. We compared our method against manual techniques and ones employed by previous researchers, and the result showed our method's usefulness in many scenarios. The open-source nature of Python and OpenCV makes our method easier to adapt and customise to fit different needs.

2020 S.-T. Yau High School Science Award

8 Acknowledgement

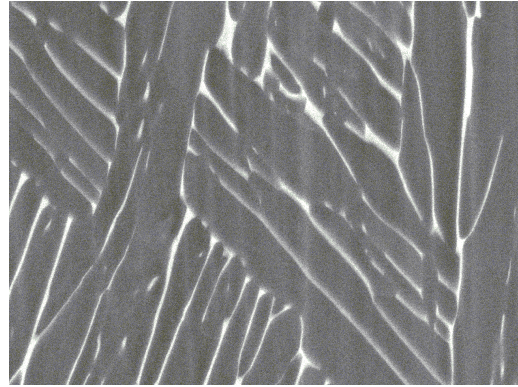
Our project idea was raised during a discussion with our supervising teacher, Dr Nathaniel Ng. We sincerely thank Dr Nathaniel for his guidance and advice. He provided many valuable suggestions on the image processing procedure and on the writing of this report. We thank Institute of Material Research and Engineering of A*STAR for providing us with the IMRE image. We are also grateful to MIPAR for allowing us to use the MIPAR image, one of the many microstructure images available on the website. Lastly, we would like to express our gratitude to Mrs Judy Tan and Mr Goh Kien Soon, both teachers from Nanyang Junior College, for providing us with the opportunity to conduct this research project with Dr Nathaniel.

2020 S.-T. Yau High School Science Award

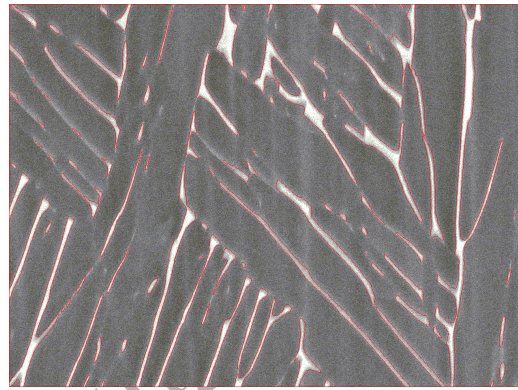
References

- [1] G. Lutjering and J. Williams, *Titanium*, ser. Engineering materials and processes. Springer, 2003. [Online]. Available: https://books.google.com.bn/books?id=GwI9ul_wAegC
- [2] A. Campbell, P. Murray, E. Yakushina, S. Marshall, and W. Ion, “New methods for automatic quantification of microstructural features using digital image processing,” *Materials & Design*, vol. 141, pp. 395–406, 2018.
- [3] A. Standard, “E112, 2013 standard test methods for determining average grain size astm international,” *West Conshohocken, PA*, 2013.
- [4] J. M. Sosa, D. E. Huber, B. Welk, and H. L. Fraser, “Development and application of mipar™: a novel software package for two-and three-dimensional microstructural characterization,” *Integrating Materials and Manufacturing Innovation*, vol. 3, no. 1, p. 10, 2014.
- [5] J. Tiley, T. Searles, E. Lee, S. Kar, R. Banerjee, J. Russ, and H. Fraser, “Quantification of microstructural features in α/β titanium alloys,” *Materials Science and Engineering: A*, vol. 372, no. 1-2, pp. 191–198, 2004.
- [6] P. C. Collins, B. Welk, T. Searles, J. Tiley, J. Russ, and H. Fraser, “Development of methods for the quantification of microstructural features in $\alpha + \beta$ -processed α/β titanium alloys,” *Materials Science and Engineering: A*, vol. 508, no. 1-2, pp. 174–182, 2009.
- [7] D. Yang and Z. Liu, “Quantification of microstructural features and prediction of mechanical properties of a dual-phase ti-6al-4v alloy,” *Materials*, vol. 9, no. 8, p. 628, 2016.
- [8] N. Otsu, “A threshold selection method from gray-level histograms,” *IEEE transactions on systems, man, and cybernetics*, vol. 9, no. 1, pp. 62–66, 1979.
- [9] T. Yang, J. Ma, S. Huang, and Q. Zhao, “A new edge detection algorithm using fft procedure,” in *Proceedings of the 3rd International Conference on Multimedia Technology (ICMT 2013)*. Springer, 2014, pp. 297–304.
- [10] F. Meyer, “Topographic distance and watershed lines,” *Signal processing*, vol. 38, no. 1, pp. 113–125, 1994.
- [11] E. Dougherty, *Mathematical Morphology in Image Processing*, ser. Optical Science and Engineering. CRC Press, 2018. [Online]. Available: <https://books.google.com.sg/books?id=pUdZDwAAQBAJ>

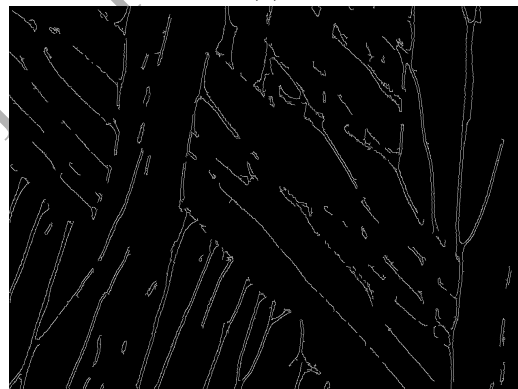
- [12] S. Beucher and F. Meyer, "The morphological approach to segmentation: the watershed transformation," *Mathematical morphology in image processing*, vol. 34, pp. 433–481, 1993.
- [13] P. P. Singhai and S. A. Ladhake, "Brain tumor detection using marker based watershed segmentation from digital mr images," *International Journal of Innovative Technology and Exploring Engineering (IJITEE) ISSN*, pp. 2278–3075, 2013.
- [14] K. Parvati, P. Rao, and M. Mariya Das, "Image segmentation using gray-scale morphology and marker-controlled watershed transformation," *Discrete Dynamics in Nature and Society*, vol. 2008, 2008.
- [15] S. Xu, H. Liu, and E. Song, "Marker-controlled watershed for lesion segmentation in mammograms," *Journal of digital imaging*, vol. 24, no. 5, pp. 754–763, 2011.
- [16] H. Breu, J. Gil, D. Kirkpatrick, and M. Werman, "Linear time euclidean distance transform algorithms," *IEEE Transactions on Pattern Analysis and Machine Intelligence*, vol. 17, no. 5, pp. 529–533, 1995.
- [17] M. B. Dillencourt, H. Samet, and M. Tamminen, "A general approach to connected-component labeling for arbitrary image representations," *Journal of the ACM (JACM)*, vol. 39, no. 2, pp. 253–280, 1992.
- [18] A. S. for Testing and P. Materials (Filadelfia, "Astm e562-11: standard test method for determining volume fraction by systematic manual point count." ASTM, 2011.
- [19] A. W. Fitzgibbon, R. B. Fisher *et al.*, *A buyer's guide to conic fitting*. University of Edinburgh, Department of Artificial Intelligence, 1996.



(a)



(b)



(c)

Figure 11: Comparison of segmentation results where (a) original IMRE image (b) segmented image using our method (c) segmented image using Canny edge detection

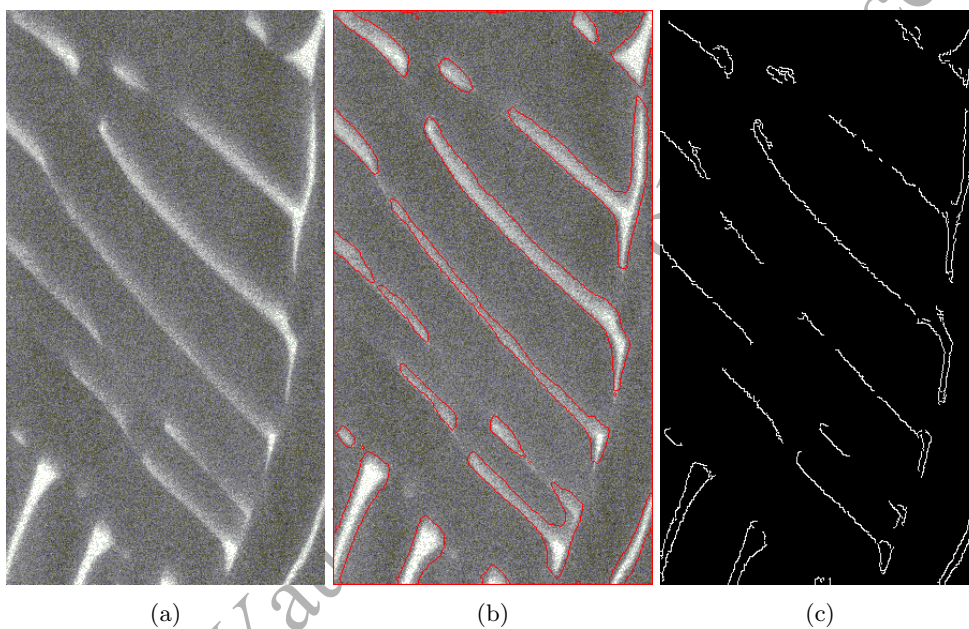
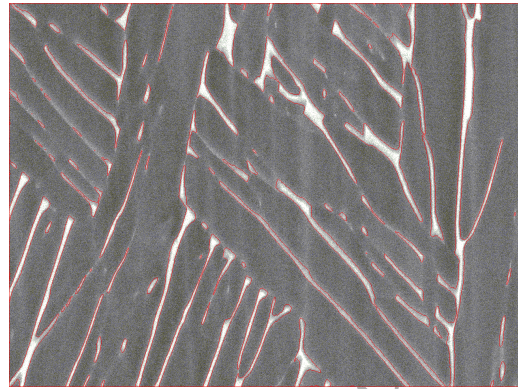
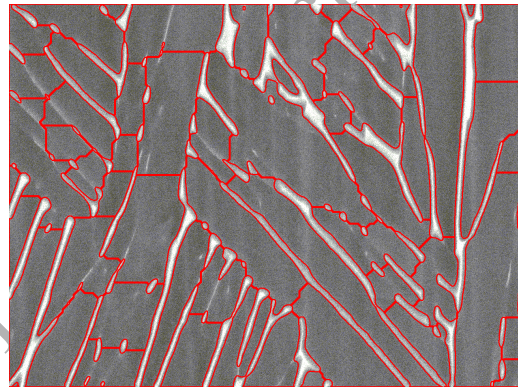


Figure 12: Comparison of segmentation results where (a) a section of the IMRE image (b) segmented section using our method (c) segmented section using Canny edge detection

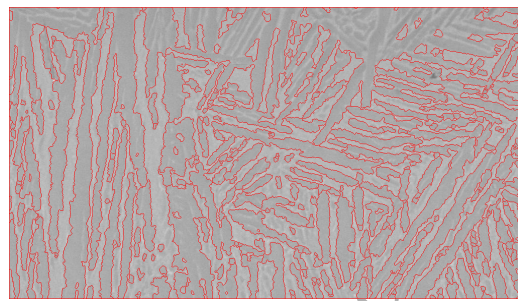


(a)



(b)

Figure 13: Comparison of segmentation results on IMRE image where (a) segmentation result using our method (b) segmented section using MIPAR software



(a)



(b)

Figure 14: Comparison of segmentation results on MIPAR image where (a) segmentation result using our method (b) segmented section using MIPAR software

Commitments on Academic Honesty and Integrity

We hereby declare that we

1. are fully committed to the principle of honesty, integrity and fair play throughout the competition.
2. actually perform the research work ourselves and thus truly understand the content of the work.
3. observe the common standard of academic integrity adopted by most journals and degree theses.
4. have declared all the assistance and contribution we have received from any personnel, agency, institution, etc. for the research work.
5. undertake to avoid getting in touch with assessment panel members in a way that may lead to direct or indirect conflict of interest.
6. undertake to avoid any interaction with assessment panel members that would undermine the neutrality of the panel member and fairness of the assessment process.
7. observe all rules and regulations of the competition.
8. agree that the decision of YHSA(Asia) is final in all matters related to the competition.

We understand and agree that failure to honour the above commitments may lead to disqualification from the competition and/or removal of reward, if applicable; that any unethical deeds, if found, will be disclosed to the school principal of team member(s) and relevant parties if deemed necessary; and that the decision of YHSA(Asia) is final and no appeal will be accepted.

(Signatures of full team below)

X

Name of team member: Xin Wenkang

X

Name of team member: Wong Zi Hao, Deston

X

Name of team member: Hoo Di Heng

X

Name of supervising teacher: Dr Nathaniel Ng

X

Name of teacher mentor: Mr Goh Kien Soon

Noted and endorsed by



Name of school principal: Mr Low Chun Meng

Low Chun Meng
Principal
Nanyang Junior College